The Fourth IEEE RAS/EMBS International Conference
on Biomedical Robotics and Biomechatronics
Roma, Italy. June 24-27, 2012

# Effect of Skin Thickness on Target Motion during Needle Insertion into Soft-Tissue Phantoms

Momen Abayazid*, Jorn op den Buijs*, Chris L. de Korte† and Sarthak Misra*
*MIRA - Institute for Biomedical Technology and Technical Medicine, University of Twente, The Netherlands
†Medical Ultrasound Imaging Center (MUSIC), Radboud University Nijmegen Medical Centre, The Netherlands

***Abstract*—Small breast lesions are increasingly detected by medical imaging modalities. However, a biopsy of the lesion is required to make a definitive diagnosis. During the biopsy, displacement of the target (lesion) occurs as the needle indents and punctures the skin layer, and penetrates further into the breast soft tissue. Target displacement during the needle insertion process makes it difficult to reach the lesion. In this study, the elastic properties of a soft-tissue phantom were estimated, and the effects of skin thickness on target motion and insertion force during needle insertion were investigated. The elastic properties of the target, skin, and the surrounding tissue were estimated *in vivo* using an ultrasound-based approach which uses "Acoustic Radiation Force Impulse" technique to determine the elastic moduli of tissue. Ultrasound images were used to track target motion during needle insertion into soft-tissue phantoms. Target displacement was computed using digital image correlation. The experimental results show that the insertion force rate increases by 90.2% and the rate of target displacement increases by 275.9%, when the skin thickness is increased from 0 mm to 2.5 mm. Studying the effect of skin thickness on the target motion during needle insertion will help in pre-operative planning and thus, improve the clinical outcomes of the biopsy procedure.**

## I. Introduction

In 2008, 458,000 women died from breast cancer worldwide [1]. Early detection and diagnosis is of key importance for effective treatment of breast cancer. After lesion detection, insertion of a biopsy needle into the breast is a frequently used procedure for diagnosis. Subsequently, samples are extracted to be screened for malignancy [2]. During needle insertion, the clinician may use ultrasound, computed tomography or magnetic resonance images to target the suspected lesion [3], [4], [5]. With advances in medical imaging, smaller breast lesions can be detected, such that accurate needle placement during biopsy becomes difficult. As the needle indents, punctures and penetrates the breast tissue, motion of the target (lesion) may occur (Figure 1). Target displacements of over 2.0 mm have been measured during breast biopsy [6].

Currently, breast biopsies are performed manually, where the clinician relies on a 'mental picture' of the needle path and target location. In some cases, target and needle locations are determined using imaging systems e.g., two-dimensional (2D) ultrasound imaging. Targeting accuracy during needle insertion could be improved by pre-operative planning of the needle insertion procedure [7]. An important part of the pre-operative plan is a patient-specific model of needle-tissue interactions [8], [9], [10], which can predict target motions. In previous studies, target displacement was expected to be due to needle-tissue interactions and the organ motion, such as in the case of respiration and fluid flow [11]. Other studies investigated the effect of the surrounding tissue elasticity, the insertion force and velocity on target motion [12], [13]. There are many factors that affect the target motion during needle insertion into soft tissue such as the organ geometry, the boundary constraints imposed by surrounding organs and connective tissue, and the mechanical properties of the surrounding tissue [8], [14]. Op den Buijs *et al.* studied the effect of different factors on the target motion during tissue indentation [15], [16]. It was observed using finite element (FE) calculations that the target displacement increases 54% when the skin thickness increases from 1.0 mm to 2.0 mm during tissue indentation. This large increase of the target displacement is expected to have a drastic effect on the targeting accuracy during the needle insertion procedure. The skin thickness of the human breast ranges from 0.8 mm to

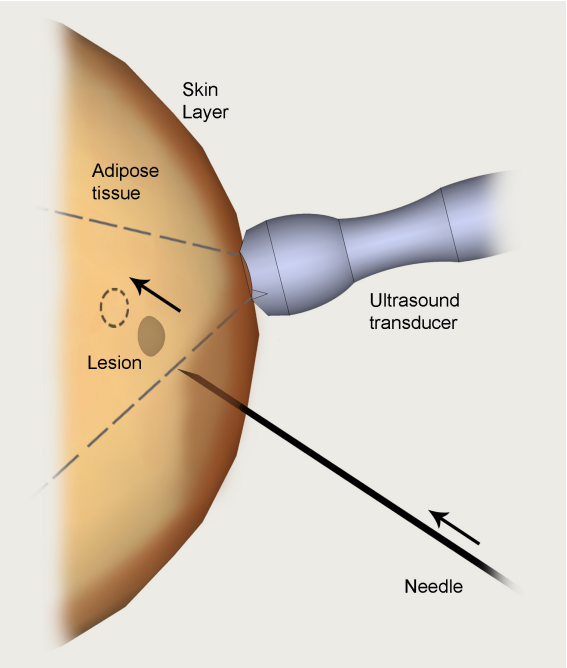


Figure 1. Schematic of an ultrasound-guided needle insertion: Interactions between needle and breast soft tissue cause target (lesion) motion.

This work was supported by funds from the Netherlands Organization for Scientific Research (NWO). The authors thank Youri van Veen and Gerben te Riet o/g Scholten for their help and advice in conducting the experiments.
Corresponding email: m.abayazid@utwente.nl

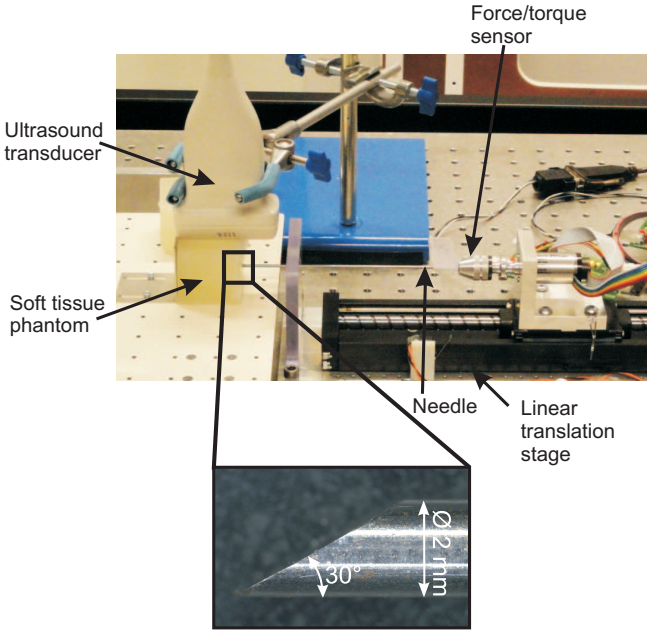


Figure 2. Photograph of the needle insertion setup with the soft-tissue phantom. A linear array ultrasound transducer is mounted on top of a phantom. A needle, mounted on a linear translation stage, was inserted into a phantom at a speed of 30 mm/s. The inset contains a microscopic photograph of a 2.0 mm diameter stainless steel needle with bevel-edged tip ($30^o$).

3.0 mm [17]. Thus, studying the influence of skin thickness on target motion is important for enhancing targeting accuracy of needle insertion.

Skin tissue is generally stiffer than adipose tissue, and thus skin penetration by the needle requires a relatively high insertion force [12]. This results in increased displacement of the adipose tissue and lesion below the skin surface. Previous work by Ophir *et al.* and Galloti *et al.* showed that it is possible to estimate soft tissue properties *in vivo* and non-invasively using ultrasound-based elasticity tools such as elastography [18], [19], [20] and acoustic radiation force impulse (ARFI) imaging [21], [22]. In this study, we use the ultrasound-based ARFI technique to estimate the elastic moduli of the adipose tissue and lesion. ARFI technique is chosen to be applied in the current study because unlike elastography it does not require inverse FE calculations [16]. The aim of non-invasively estimating the mechanical properties of different tissue layers is to predict tissue deformation during needle insertion.

In this paper, we investigate the influence of the skin thickness on the target motion during needle insertion into soft-tissue phantoms. Soft-tissue phantoms used in the experiments were made of layers representing skin and adipose tissue which contains the lesion. The phantom was made of gelatin and silicone rubber to model the mechanical properties of breast tissue [23]. The influence of the skin layer was investigated by testing phantoms without skin layer and with skin layer of different thicknesses. The needle insertion force rate was measured during the experiments, and the target displacement was detected. Several techniques were integrated to investigate the effect of the skin thickness on the target motion during needle insertion. An ultrasound-based ARFI technique is used to estimate the elastic modulus of the target and the surrounding tissue. Digital image correlation (DIC) algorithm was applied on B-mode ultrasound images to estimate the target motion. Insertion force rate and velocity were measured during the experiments to determine the relation between the skin thickness and the target motion.

This paper is organized as follows: Section II describes the technique used to estimate the elastic modulus of a soft-tissue phantom from ultrasound measurements. Section III explains the preparation of tissue phantoms, the experimental setup used for needle insertion experiments, and the algorithm used to track the target motion. Section IV discusses the experimental results, followed by conclusions and future work.

## II. Elasticity of Soft-Tissue Phantom

Ultrasound-based ARFI technique was used to determine the elastic moduli of the silicone rubber (target and skin) and gel (adipose tissue). The soft-tissue phantom preparation is described in the next section (Section III-A). The Young's modulus is estimated using a commercially available implementation of ARFI technology, or known as Virtual Touch™ Quantification, installed on a Siemens Acuson S2000 ultrasound machine (Siemens AG, Erlangen, Germany). ARFI is a quantitative technique to estimate the tissue elasticity by measuring the velocity of the shear wave. Shear waves are generated by displacement of tissue. These waves are detected by the ultrasound transducer and the shear velocity is measured. Virtual Touch™ Quantification provides the shear wave velocity for the defined region of interest using the linear array transducer 9L4. The target and gel are assumed to be isotropic and incompressible. Young's modulus ($E$) in different regions is calculated as [22]

$$G = \rho v_s^2, \tag{1}$$

where $G$ and $v_s$ are the shear modulus and the shear wave propagation velocity, respectively. The density ($\rho$) of the material is calculated from the mass and volume of the soft-tissue phantom and the target. Young's modulus ($E$) is calculated by

$$E = 2G(1+\gamma), \tag{2}$$

where $\gamma$ is Poisson's ratio which is assumed to be 0.495.

## III. Experimental Setup

In this section, the phantom preparation method is described. The experimental setup and the components used in the needle insertion measurements are presented. The algorithm used for tracking the target motion is also illustrated in this section.

### A. Soft-tissue phantom preparation

The adipose tissue, lesion and skin layer were needed to be represented in the soft-tissue phantom. Gelatin mixture was used to simulate the adipose tissue. Silicone rubber was used to mimic the properties of the lesion and the skin layer [15]. Gelatin (8.0%-by-weight) (Dr. Oetker, Ede, The Netherlands),

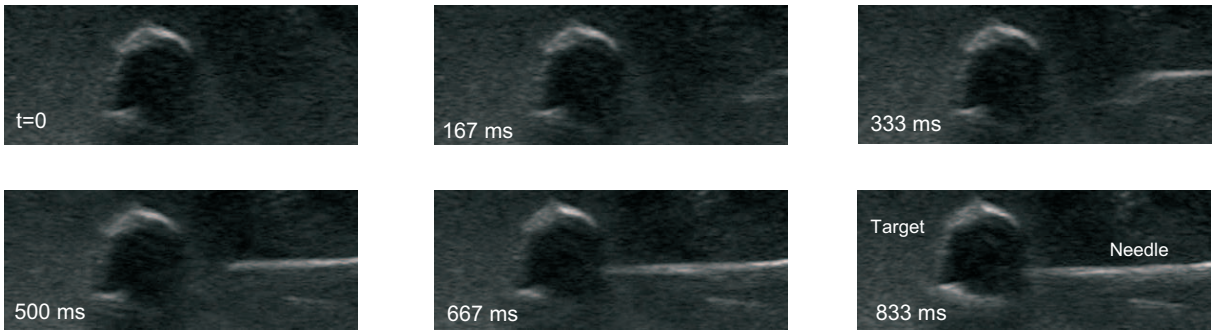


Figure 3. Frames of ultrasound images during needle insertion into phantom with no skin layer.

and silica gel (1.0%-by-weight) (particle size $< 63\,\mu$m SiC, E. Merck, Darmstadt, Germany) were mixed with boiling water. The silica gel served to mimic tissue acoustic scattering. The mixture was then put in a plastic container ($46 \times 28 \times 71$ mm³). Small beads of silicone rubber (8.0 mm diameter) were used to model the stiff targets. Silicone rubber beads were positioned in the gelatin solution by hanging them using thin wires. The gel solidifies after one hour at temperature of 7°C. The wires that suspend the rubber beads are removed, and the phantoms are taken out of the container. The last step is to add the silicone layer (skin) on the phantom, and allow the layer to solidify at room temperature. We prepared three sets of phantoms. The first set consists of phantoms without skin layer. The second and third sets consist of phantoms with skin layers of 1.5 mm and 2.5 mm thickness, respectively. To measure skin thickness, B-mode ultrasound images of the phantom were recorded by a Philips HD 11XE ultrasound system (Philips Medical Systems, Best, The Netherlands), equipped with a linear array ultrasound transducer (L12-5). The phantoms used in elasticity measurements (Section II) and in the needle insertion experiments (Section III-B) were made of the same materials.

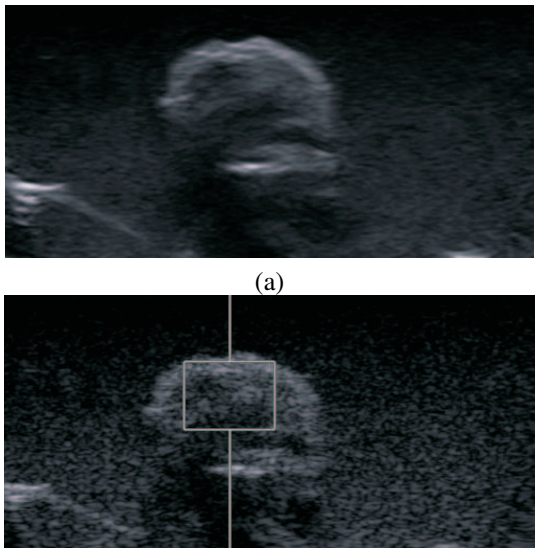

(a)

(b)

Figure 4. Elastic moduli calculation: (a) The ultrasound image shows the target shape. The rectangle in (b) represents the region of interest where ultrasound-based ARFI is applied.

### *B. Needle insertion experiments*

The experimental setup used for needle insertion into the tissue phantom is shown in Figure 2. A stainless steel needle (2.0 mm diameter) with bevel tip ($30^o$) is used in the experiments. The insertion process was performed by placing the needle into a sub-assembly mounted on a linear translation stage (Misumi Group Inc., Tokyo, Japan). The linear stage was actuated by a DC motor with planetary gear-head with transmission ratio of 4.4:1 and optical encoder (Maxon Motor AG, Sachseln, Switzerland), which was operated by a controller (Elmo Motion Control Ltd., Petach-Tikva, Israel). The needle insertion axis was positioned perpendicular to the skin layer plane of the tissue phantom. The needle was then inserted into the phantom at a speed of 30 mm/s [24]. The insertion distance was 30.0 mm. A six degrees of freedom (DOF) ATI nano17 force/torque sensor (ATI Industrial Automation, Apex, USA) was fixed at the base of the needle to record the forces acting on the needle during insertion. B-mode ultrasound images of the target were recorded at 15 frames per second to track the needle insertion and target motion. The ultrasound transducer was fixed by a clamp and positioned on top of the phantom touching its upper surface, such that the stiff target was in the field of view.

### *C. Target motion tracking*

Ultrasound images with $0.09 \times 0.09$ mm$^2$ pixels were exported to Matlab (v7.11, Mathworks Inc., Natick, USA) for processing. Ultrasound image frames of needle insertion into soft-tissue phantom are shown in Figure 3 to depict the geometry of the needle and the target in the ultrasound images. The target displacement was tracked using DIC algorithm. The DIC algorithm used 2D cross-correlation of a square of $15 \times 15$ pixels around pixel coordinates $(x_k, y_k)$ in frame $k$ with a square of $30 \times 30$ pixels in frame $k + \Delta k$. The peak location of the correlation values was detected by parabolic interpolation, resulting in determination of $(x_{k+\Delta k}, y_{k+\Delta k})$ with sub-pixel resolution. Steps of $\Delta k = 2$ frames were used. The target motion $(u_k, v_k)$ was calculated as $(x_k - x_0, y_k - y_0)$ where $(x_0, y_0)$ is the initial pixel coordinates selected at the first frame. The total displacement $(U_k)$ was calculated as $U_k = \sqrt{u_k^2 + v_k^2}$.

Table I

THE SHEAR VELOCITY ($v_s$) WAS MEASURED AT DIFFERENT LOCATIONS IN THE GEL AND THE TARGET (FIVE TRIALS EACH) TO MEASURE THE ELASTIC MODULI ($E$). THE *Mean* IS THE AVERAGE VALUE OF THREE EXPERIMENTS PERFORMED FOR EACH CASE, AND *SD* IS THE STANDARD DEVIATION.

| $v_s$ (m/s) | | | | $\rho$ (kg/m$^3$) | | $G$ (kPa) | | $E$ (kPa) | |
|---|---|---|---|---|---|---|---|---|---|
| Target | | Gel | | Target | Gel | Target | Gel | Target | Gel |
| *Mean* | *SD* | *Mean* | *SD* | 2619.86 | 925.63 | 79.25 | 11.11 | 237 | 33.21 |
| 5.5 | 0.42 | 3.46 | 0.16 | | | | | | |

## IV. RESULTS

In this section, the results of the elasticity measurements are discussed, and the elastic moduli of the soft-tissue phantom and the target are presented. The experimental results of target displacement and insertion forces during needle insertion into soft-tissue phantoms with different skin thicknesses are also presented.

### A. Elastic modulus

The elastic moduli ($E$) of the target and the gel are measured using the ultrasound-based ARFI technique as mentioned in Section II. The shape of the target in the ultrasound image is shown in Fig 4. The shear velocity ($v_s$) is measured five times for repeatability. The parameters used for calculating the elastic moduli are tabulated in Table I.

### B. Insertion force and target displacement

Using the needle insertion setup described in Section III-B, needle insertion experiments were performed. Ultrasound was used to image the needle insertion process and to detect the target motion during the insertion procedure. Ultrasound measurements were recorded for three experimental cases:

- Case 1: The needle was inserted into phantoms with no skin layer.
- Case 2: The needle was inserted into phantoms with 1.5 mm skin layer.
- Case 3: The needle was inserted into phantoms with 2.5 mm skin layer.

For each case, $n = 3$ experiments were performed on the same phantom to determine the repeatability of the insertion experiments. In order to eliminate the error that may arise due to inaccuracy in the placement of the target into the phantom during gel preparation, the rate of force and displacement increase were used in the measurements instead of the peak force and velocity to determine the effect of the skin thickness on the target motion during needle insertion.

During the needle insertion process, the needle passes through three stages, as shown in Figures 5 and 6. The first stage (I) starts when the needle penetrates the skin layer and ends just before reaching the target. In the second stage (II), the needle interacts with the target by penetrating it, and then proceeding to the soft-tissue phantom again. In the last stage (III), the needle motion stops, and the phantom relaxes and moves opposite to the direction of needle penetration. As shown in Figure 5, in the first stage (I), the insertion force increases as the needle tip penetrates the soft-tissue phantom for the three cases. The slope of the insertion force curve in the first stage (I) shows the rate of force increase during needle penetration (Table II). The slope is calculated after fitting all the data points to a linear polynomial using Matlab (v7.11, Mathworks Inc., Natick, USA) curve fitting tool box. The insertion force increases at a higher rate when the needle is inserted into phantoms with thicker skin layers. In the second stage (II), the needle tip penetrates the target, and then it penetrates the soft-tissue phantom again. The needle interaction with the target, and the motion of the needle tip from one medium to another results in fluctuations of the force curves. In the last stage (III), when the motion stops, the force decreases smoothly because the phantom relaxes and applies force on the needle opposite to the direction of penetration.

The experimental results of the target displacement during needle insertion are shown in Figure 6. In the first stage (I), the target displacement increases in the direction of penetration as the needle tip moves closer to the target. The slopes of the target displacement curves show that the rate of increase of target displacement in the first stage is dependent on the skin thickness (Table II). In the second stage (II), the needle tip pushes the target, and then penetrates it, and that causes target displacement in the direction of needle penetration. In the last stage (III), the needle stops, and the displaced volume of the phantom moves back opposite to the direction of needle penetration. The measurements show that the target displacement is maximum for Case 3 and minimum for Case 1. The needle insertion stages are illustrated in Figures 5 and 6, and an ultrasound image frame is attached to each stage for clarification.

### C. Discussion

The results presented in Figures 5 and 6 show that thicker skin results in higher rates of insertion force and target displacement. The experimental results show that thick skin layer (2.5 mm) causes 90.3% increase in the insertion force rate compared to a phantom with no skin layer (Table II). The rate of target displacement increases 275.9% when the needle is inserted into a phantom with thick skin layer (2.5 mm) compared to a phantom with no skin layer. These results indicate the significance of modeling skin, since breast skin thickness ranges from 0.8 mm to 3.0 mm [17]. This range is large enough to affect the target motion during needle insertion. Consequently, it is recommended to measure the elasticity and thickness of the soft tissue layers before biopsy for accurate prediction of the target motion during needle insertion.

## V. CONCLUSIONS AND FUTURE WORK

In this study, we focused on studying the effects of the skin thickness on the insertion force rate and the target motion during needle insertion into soft-tissue phantom. The elasticity

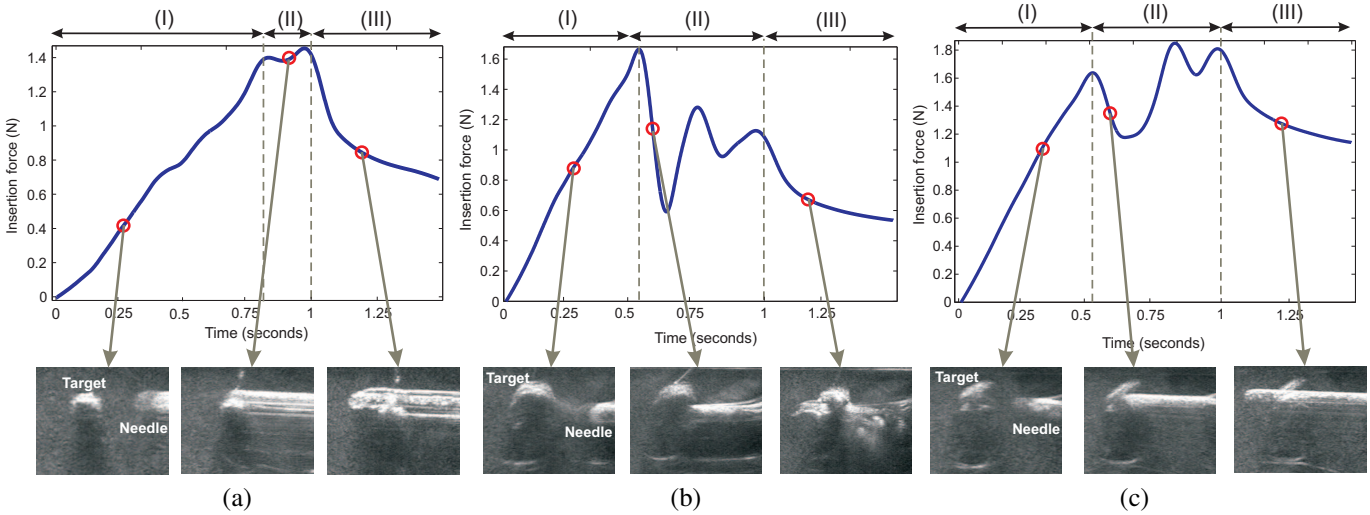


Figure 5. Insertion force measured during insertion of the needle into phantoms with: (a) no skin layer (Case 1), (b) 1.5 mm skin layer (Case 2) and (c) 2.5 mm skin layer (Case 3). The insertion stages are represented by: (I) before reaching the target, (II) needle-target interaction and (III) stopping the insertion and phantom relaxation.

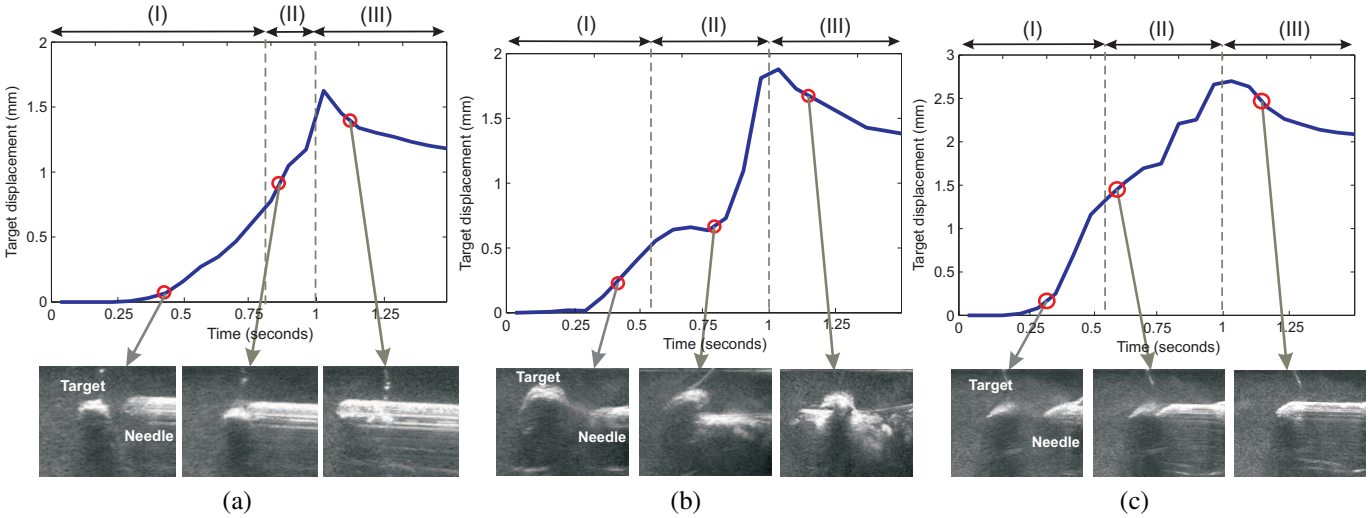


Figure 6. Target displacement measured during insertion of the needle into phantoms with: (a) no skin layer, (b) 1.5 mm skin layer and (c) 2.5 mm skin layer. The insertion stages are represented by: (I) before reaching the target, (II) needle-target interaction and (III) stopping the insertion and phantom relaxation.

Table II
EXPERIMENTAL RESULTS FOR THE INSERTION FORCE AND THE TARGET DISPLACEMENT RATES IN STAGE (I).

| | | **Insertion force per unit time (N/s)** | | **Target displacement per unit time (mm/s)** | |
|---|---|---|---|---|---|
| | | *Mean* | *SD* | *Mean* | *SD* |
| **No skin** | Case 1 | 1.95 | 0.23 | 0.54 | 0.11 |
| **1.5 mm skin** | Case 2 | 3.50 | 0.29 | 1.31 | 0.20 |
| **2.5 mm skin** | Case 3 | 3.71 | 0.36 | 2.03 | 0.57 |

of the target and the surrounding gel were estimated non-invasively using ultrasound-based ARFI technique. DIC algorithm was used to calculate the target motion during needle insertion. It is concluded from the experiments that increasing the skin thickness leads to higher insertion force rates and larger target displacement rates during needle insertion.

Target motion can be also affected by other factors such as needle insertion speed, needle diameter and shape of needle tip. These factors will be investigated in future studies using needle insertion setup. Ultrasound-based ARFI technology provides an estimation of the elastic moduli of the adipose tissue and target non-invasively. The elastic moduli can be used as inputs to FE models that compute the target motion and tissue deformation during needle insertion into soft tissue. Prediction of the target motion will improve the accuracy of pre-operative needle path planning. In the current study, the target displacement was tracked in two dimensions, and for future work the displacement of the target will be measured in three dimensions [25], [26]. Pre-operative needle path planning and three-dimensional tracking of the target displacement in real time will assist in increasing the targeting accuracy during needle insertion procedures such as biopsies.

## REFERENCES

[1] J. Ferlay, H. R. Shin, F. Bray, D. Forman, C. Mathers, and D. M. Parkin, "Cancer incidence and mortality worldwide." International Agency for Research on Cancer, 2010.

[2] M. Guray and A. A. Sahin, "Benign breast diseases: Classification, diagnosis, and management," *Oncologist*, vol. 11, no. 5, pp. 435–449, 2006.

[3] W. A. Kaiser, S. O. R. Pfleiderer, and P. A. T. Baltzer, "MRI-guided interventions of the breast," *Journal of Magnetic Resonance Imaging*, vol. 27, no. 2, pp. 347–355, 2008.

[4] G. Schueller, C. Schueller-Weidekamm, and T. H. Helbich, "Accuracy of ultrasound-guided, large-core needle breast biopsy," *European Radiology*, vol. 18, no. 9, pp. 1761–1773, 2008.

[5] R. G. Stock and N. N. Stone, "Current topics in the treatment of prostate cancer with low-dose-rate brachytherapy," *Urologic Clinics of North America*, vol. 37, no. 1, pp. 83–96, 2010.

[6] E. E. Deurloo, K. G. Gilhuijs, L. J. Schultze Kool, and S. H. Muller, "Displacement of breast tissue and needle deviations during stereotactic procedures," *Investigative Radiology*, vol. 36, no. 6, pp. 347–353, 2001.

[7] N. Abolhassani, R. Patel, and M. Moallem, "Needle insertion into soft tissue: a survey," *Medical Engineering & Physics*, vol. 29, no. 4, pp. 413–431, 2007.

[8] S. Misra, K. T. Ramesh, and A. M. Okamura, "Modeling of tool-tissue interactions for computer-based surgical simulation: a literature review," *Presence: Teleoperators and Virtual Environments*, vol. 17, no. 5, pp. 463–491, 2008.

[9] S. P. DiMaio and S. E. Salcudean, "Interactive simulation of needle insertion models," *IEEE Transactions on Biomedical Engineering*, vol. 52, no. 7, pp. 1167–1179, 2005.

[10] E. Dehghan, X. Wen, R. Zahiri-Azar, M. Marchal, and S. E. Salcudean, "Modeling of needle-tissue interaction using ultrasound-based motion estimation," in *Medical Image Computing and Computer-Assisted Intervention, MICCAI* (N. Ayache, S. Ourselin, and A. Maeder, eds.), vol. 4791 of *Lecture Notes in Computer Science*, pp. 709–716, Springer Berlin / Heidelberg, 2007.

[11] J.-S. Hong, T. Dohi, H. Makoto, K. Konishi, and N. Hata, "A motion adaptable needle placement instrument based on tumor specific ultrasonic image segmentation," in *proceedings of the 5th International Conference on Medical Image Computing and Computer-Assisted Intervention-Part I*, MICCAI, (London, UK), pp. 122–129, Springer-Verlag, 2002.

[12] S. Badaan, D. Petrisor, C. Kim, P. Mozer, D. Mazilu, L. Gruionu, A. Patriciu, K. Cleary, and D. Stoianovici, "Does needle rotation improve lesion targeting?," *The International Journal of Medical Robotics and Computer Assisted Surgery*, vol. 7, no. 2, pp. 138–147, 2011.

[13] H. Xu, A. Lasso, S. Vikal, P. Guion, A. Krieger, A. Kaushal, L. Whitcomb, and G. Fichtinger, "Mri-guided robotic prostate biopsy: A clinical accuracy validation," in *Medical Image Computing and Computer-Assisted Intervention (MICCAI)* (T. Jiang, N. Navab, J. Pluim, and M. Viergever, eds.), vol. 6363, pp. 383–391, Springer Berlin / Heidelberg, 2010.

[14] S. Misra, K. J. Macura, K. T. Ramesh, and A. M. Okamura, "The importance of organ geometry and boundary constraints for planning of medical interventions," *Medical Engineering & Physics*, vol. 31, no. 2, pp. 195–206, 2009.

[15] J. op den Buijs, M. Abayazid, C. L. de Korte, and S. Misra, "Target motion predictions for pre-operative planning during needle-based interventions," in *proceedings of the Annual International Conference of the IEEE Engineering in Medicine and Biology Society (EMBS)*, (Boston, USA), pp. 5380–5385, August-September 2011.

[16] J. op den Buijs, H. H. G. Hansen, R. G. P. Lopata, C. L. de Korte, and S. Misra, "Predicting target displacements using ultrasound elastography and finite element modeling," *IEEE Transactions on Biomedical Engineering*, vol. 58, no. 11, pp. 3143 –3155, 2011.

[17] S. Willson, E. Adam, and A. Tucker, "Patterns of breast skin thickness in normal mammograms," *Clinical Radiology*, vol. 33, no. 6, pp. 691–693, 1982.

[18] T. Hall, A. Oberait, P. Barbone, A. Sommer, N. Gokhale, S. Goenezent, and J. Jiang, "Elastic nonlinearity imaging," in *proceedings of the 31st Annual International Conference of the IEEE Engineering in Medicine and Biology Society (EMBS)*, (Minneapolis, USA), pp. 1967–1970, 2009.

[19] T. R. Kumm and M. M. Szabunio, "Elastography for the characterization of breast lesions: initial clinical experience," *Cancer Control*, vol. 17, no. 3, pp. 156–161, 2010.

[20] J. Ophir, I. Céspedes, H. Ponnekanti, Y. Yazdi, and X. Li, "Elastography: a quantitative method for imaging the elasticity of biological tissues," *Ultrasonic Imaging*, vol. 13, no. 2, pp. 111–134, 1991.

[21] A. Gallotti, M. D'Onofrio, and R. Pozzi Mucelli, "Acoustic radiation force impulse (ARFI) technique in ultrasound with virtual touch tissue quantification of the upper abdomen," *La Radiologia Medica*, vol. 115, no. 6, pp. 889–897, 2010.

[22] M. L. Palmeri, M. H. Wang, J. J. Dahl, K. D. Frinkley, and K. R. Nightingale, "Quantifying hepatic shear modulus in vivo using acoustic radiation force.," *Ultrasound in medicine biology*, vol. 34, no. 4, pp. 546–558, 2008.

[23] M. O. Culjat, D. Goldenberg, P. Tewari, and R. S. Singh, "A review of tissue substitutes for ultrasound imaging," *Ultrasound in Medicine & Biology*, vol. 36, no. 6, pp. 861–873, 2010.

[24] T. Podder, D. Clark, D. Fuller, J. Sherman, W. Ng, L. Liao, D. Rubens, J. Strang, E. Messing, Y. Zhang, and Y. Yu, "Effects of velocity modulation during surgical needle insertion," in *proceedings of the 27th Annual International Conference of the IEEE Engineering in Medicine and Biology Society (EMBS)*, (San Francisco, USA), pp. 5766–5770, 2005.

[25] Z. Wei, L. Gardi, D. B. Downey, and A. Fenster, "Oblique needle segmentation and tracking for 3d trus guided prostate brachytherapy," *Medical Physics*, vol. 32, pp. 2928 – 2941, 2005.

[26] G. Fichtinger, J. P. Fiene, C. W. Kennedy, G. Kronreif, I. Iordachita, D. Y. Song, E. C. Burdette, and P. Kazanzides, "Robotic assistance for ultrasound-guided prostate brachytherapy," *Medical Image Analysis*, vol. 12, no. 5, pp. 535–545, 2008.